

Stability Analysis of Magnetoconvection in a Fluid-Porous System with Thermal Effects

Anil Kumar¹, and D. Bhargavi²

^{1,2}Department of Mathematics, National Institute of Technology, Warangal, Telangana 506004, India

*E-mail: ak21marer01@student.nitw.ac.in

Abstract - This study investigates the linear and nonlinear stability analysis of thermal convection in a fluid layer overlying a highly porous material, subjected to a vertical magnetic field and maintained at a constant wall temperature. A two-layer approach is adopted, where the Darcy-Brinkman model is used to describe fluid flow within the porous medium. The influence of the magnetic field on both linear and nonlinear stability is analysed. The Chebyshev-Tau-QZ spectral method is employed to solve the coupled ordinary differential equations, formulated as an eigenvalue problem. This approach is particularly advantageous for fluid-porous convection problems due to its high accuracy. Nonlinear stability analysis is conducted using the energy method, and the results are validated against existing literature. The magnetic field shows stabilizing effect and with increase in depth ratio also revealed stabilizing effect. The findings of this study have significant applications in geophysical fluid dynamics, magnetohydrodynamics, and industrial processes such as thermal insulation, cooling systems, and crystal growth, where heat transfer in porous-fluid systems plays a critical role.

Keywords: Darcy-Brinkman model, porous media, Chebyshev-Tau-QZ spectral method

1. Introduction

This study investigates the growth and evolution of both infinitesimal and finite disturbances in a channel where a free fluid layer overlies a porous medium, with no-slip at the walls, constant-temperature boundaries, and a transverse magnetic field. Such configurations are found in MHD heat exchangers, microfluidic thermal-management systems, and electromagnetically enhanced oil recovery, where accurately predicting the onset of convection (via critical Rayleigh and Hartmann numbers) and its subsequent nonlinear development is crucial for safe, efficient operation. By elucidating how slip length, permeability contrasts, and magnetic damping jointly influence stability, this work bridges pore-scale Darcy-Brinkman dynamics and bulk flow behaviour, providing actionable guidelines to delay transition, maximize heat transfer, and inform geophysical and industrial designs. As a result, the study of channels partially filled with porous media has gained significant attention, leading to a variety of investigations due to their relevance in numerous industrial and geophysical applications [1–6]. Among these, A.A. Hill and B. Straughan [7,8] adopted a dual-layer approach based on the Darcy-Brinkman model to describe fluid flow through the porous medium. Their formulation included a tangential stress jump condition at the interface between the clear fluid and the porous region, making it suitable for modeling high-porosity materials such as metal foams commonly used in heat exchangers and fluid filtration systems.

Hill and Straughan [9,10] studied the stability of Poiseuille flow in a three-layer system fluid, Brinkman transition, and Darcy porous layers identifying two key instability modes influenced by layer depths and transition thickness. The Brinkman layer notably suppressed a third mode seen in simpler models. Numerical results aligned with previous studies. Additionally, the magnetic field plays a crucial role in the onset and control of convection by exerting a damping force (Lorentz force) that stabilizes fluid motion. In this study, we consider the effect of a vertical magnetic field on a fluid overlying a porous medium, as such configurations are relevant in numerous engineering and geophysical applications, including nuclear reactors, crystal growth, MHD generators, and groundwater flow in magnetized environments [11].

2. Mathematical model

The mathematical model is shown in Fig. 1 and it is shown that both walls are kept at constant wall temperature with no slip wall conditions and vertical magnetic field is applied to a channel where fluid overlying a porous medium.

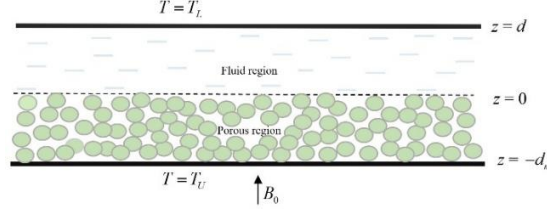


Fig. 1: Schematic physical model

2.1. Governing equations

Fluid Region ($d \leq z \leq 0$)

Equation of continuity

$$\frac{\partial u_i^f}{\partial x_i} = 0 \quad (1)$$

Conservation of momentum [8]

$$\rho_0 \frac{\partial u_i^f}{\partial t} = -\frac{\partial p^f}{\partial x_i} + \mu \Delta u_i^f - g \rho_0 \hat{k} (1 - \alpha (T^f - T_0)) + J^f \times B \quad (2)$$

$$J^f = \sigma_1 (u_i^f \times B) \text{ where } B = B_0 \hat{k} \quad (3)$$

In Eq. (3) J^f is the current density and σ_1 is the electrical conductivity.

Conservation of Energy [8]

$$\frac{\partial T^f}{\partial t} + u_i^f \frac{\partial T^f}{\partial x_i} = \frac{K^f}{(\rho_0 c_p)_f} \nabla^2 T^f \quad (4)$$

Porous Region ($-d_m \leq z \leq 0$)

Equation of continuity

$$\frac{\partial u_i^m}{\partial x_i} = 0 \quad (5)$$

Conservation of momentum [8]

$$\frac{\rho_0}{\phi} \frac{\partial u_i^m}{\partial t} = -\frac{\partial p^m}{\partial x_i} + \mu_e \Delta u_i^m - \frac{\mu}{K} u_i^m - g \rho_0 \hat{k} (1 - \alpha (T^m - T_0)) + J^m \times B \quad (6)$$

$$J^m = \sigma_1 (u_i^m \times B) \text{ where } B = B_0 \hat{k} . \quad (7)$$

In Eq. (7) J^m is the current density for porous region.

Conservation of Energy [8]

$$\frac{(\rho_0 c_p)_m}{(\rho_0 c_p)_f} \frac{\partial T^m}{\partial t} + u_i^m \frac{\partial T^m}{\partial x_i} = \frac{K^m}{(\rho_0 c_p)_f} \nabla^2 T^m \quad (8)$$

Boundary conditions [8]

$$T = T_U, u_i = u_{3,3} = 0 \text{ at } z = d \quad (9)$$

$$T = T_L, u_i^m = u_{3,3}^m = 0 \text{ at } z = -d^m \quad (10)$$

Where $T_L > T_U$ and at interfacial conditions at porous and fluid at $z = 0$

$$u_i^f = u_i^m, T^f = T_m \text{ and } K^f \frac{\partial T^f}{\partial z} = K^m \frac{\partial T^m}{\partial z} \quad (11)$$

Continuity of normal stresses

$$-p + 2\mu \frac{\partial u_3}{\partial z} = -p^m + \frac{2\mu}{\phi} \frac{\partial u_3^m}{\partial z} \quad (12)$$

Continuity of tangential stresses

$$\mu \left(\frac{\partial u_\gamma}{\partial z} + \frac{\partial u_3}{\partial x_\gamma} \right) = \frac{\mu}{\phi} \left(\frac{\partial u_\gamma^m}{\partial z} + \frac{\partial u_3^m}{\partial x_\gamma} \right), \text{ where } \gamma = 1, 2 \quad (13)$$

In Eqs. (1)-(13), u_i^f, p^f, T^f, t are velocity, pressure, temperature, and time in the fluid region, μ is the dynamic viscosity, d is the width of fluid region, β is Casson Parameter, $B = B_0 \hat{k}$ is a magnetic field, α is coefficient of thermal expansion, g is the acceleration due to gravity, T_0 is reference temperature, ρ_0 is the reference density, $x_i = (x, y, z)$, \hat{k} is unit vector, u_i^m, p^m, T^m are velocity, pressure, temperature in porous region, K^f is the thermal conductivity in fluid region, d_m is the width of porous region, c_p is heat capacity, ϕ is porosity, K^m is the thermal conductivity in porous region, μ_e is the effective viscosity and is defined as $\mu_e = \frac{\mu}{\phi}$,

2.2. Perturbation method

To evaluate the stability of the steady-state solution, we apply small perturbations to it, such that

$$u_i^f = u_b^f + \bar{u}_i^f, T^f = T_b^f + \bar{\theta}^f, p^f = p_b^f + \bar{p}^f \quad (14)$$

$$u_i^m = u_b^m + \bar{u}_i^m, T^m = T_b^m + \bar{\theta}^m, p^m = p_b^m + \bar{p}^m \quad (15)$$

Non-dimensional variables

$$u_i^f = \frac{\mu}{\rho_0 d} \bar{u}_i^f, p^f = \frac{\mu^2}{\rho_0 d^2} \bar{p}^f, \theta^f = \bar{\theta}^f \sqrt{\frac{\mu^3 (T_L - T_U)}{\rho_0^3 g \alpha d^3 K^f}}, x_i = \bar{x}_i d, t = \frac{d^2}{\nu} \bar{t} \quad (16)$$

2.3. Base state solutions

The base state velocity and temperature in fluid and porous regions are defined as follows

$$u_b^f = 0 \quad (17)$$

$$T_b^f = -\frac{(T_L - T_U)z}{d_m(\epsilon_T + d_r)} + \frac{d_r T_L + \epsilon_T T_U}{(\epsilon_T + d_r)}, z \in (0, d) \quad (18)$$

$$u_b^m = 0 \quad (19)$$

$$T_b^m = -\frac{\epsilon_r (T_L - T_U) z}{d_m (\epsilon_r + d_r)} + \frac{d_r T_L + \epsilon_r T_U}{(\epsilon_r + d_r)}, z \in (-d_m, 0) \quad (20)$$

$$\text{where, } \epsilon_r = \frac{K^f}{K^m}, d_r = \frac{d}{d_m} \quad (21)$$

In Eq. (21) d_r is the depth ratio. The governing Eqs. (1) -(13) are non-dimensionalized with given scaling parameters in Eq. (16). The non-dimensional form of governing equations is obtained after using a non-dimensional variable in Eqs. (1) -(13) are

Fluid region ($1 \leq z \leq 0$)

$$\frac{\partial \bar{u}_i^f}{\partial x_i} = 0 \quad (22)$$

$$\frac{\partial \bar{u}_i^f}{\partial \bar{t}} = -\frac{\partial \bar{p}^f}{\partial \bar{x}_i} + \Delta \bar{u}_i^f + \bar{\theta}^f R^f \mathbf{k} + Ha^2 (\bar{u}_i^f \times \mathbf{k}) \times \mathbf{k} \quad (23)$$

$$Pr \left(\frac{\partial \bar{\theta}^f}{\partial \bar{t}} + \bar{u}_i^f \frac{\partial \bar{\theta}^f}{\partial \bar{x}_i} \right) = \bar{w}^f M_1 R^f + \Delta \bar{\theta}^f \quad (24)$$

Porous region ($-1 \leq z \leq 0$)

$$\frac{\partial \bar{u}_i^m}{\partial x_i} = 0 \quad (25)$$

$$\frac{1}{\phi} \frac{\partial \bar{u}_i^m}{\partial \bar{t}} = -\frac{\partial \bar{p}^m}{\partial \bar{x}_i} + \frac{\Delta \bar{u}_i^m}{\phi} - \frac{1}{Da} \bar{u}_i^m + R^m \bar{\theta}^m \mathbf{k} + Ha_m^2 (\bar{u}_i^m \times \mathbf{k}) \times \mathbf{k} \quad (26)$$

$$Pr \epsilon_r \left(M \frac{\partial \bar{\theta}^m}{\partial \bar{t}} + \bar{u}_i^m \frac{\partial \bar{\theta}^m}{\partial \bar{x}_i} \right) = \bar{w}^m M_2 R^m + \Delta \bar{\theta}^m \quad (27)$$

$$Ha = B_0 d \sqrt{\frac{\sigma_1}{\mu}}, Da = \frac{K}{d_m^2}, Ha_m = B_0 d_m \sqrt{\frac{\sigma_1}{\mu}}, Ha_m = \frac{Ha}{d_r}, Pr = \frac{\mu}{K^f \rho_0} \quad (28)$$

In Eq. (23)-(28), Ha and Ha_m are Hartmann numbers in fluid and porous regions, Da is Darcy number, Pr is Prandtl number, R^f is Rayleigh number in fluid region, R^m is Rayleigh number in porous region, ϵ_r , M_1 and M_2 are define as, ,

$$\epsilon_r = \frac{K^f}{K^m}, M_1 = \frac{d_r}{(d_r + \epsilon_r)}, M_2 = \frac{\epsilon_r}{(d_r + \epsilon_r)} \text{ and } R^f = \sqrt{\frac{g \alpha \rho_0 d^3 (T_L - T_U)}{\mu K^f}}.$$

2.4. Stability analysis

Although linear instability analyses provide useful insights into the initiation of convection, they may fail to detect subcritical instability cases where convection starts before the thresholds predicted by linear theory. By measuring the discrepancy between the linear instability threshold and the nonlinear stability limit, one can assess how accurately and reliably linear theory predicts the onset of convection.

2.5. Linear stability analysis

The linearized equations are derived from Eqs. (23)- (27) by discarding the nonlinear terms and taking a double curl of Eqs. (23) and (26), and eliminating the pressure term, taking out the third component assuming normal modes [12] of the form

$$\begin{aligned}\bar{u}_i^f &= u_i^f(\bar{z}) \exp(\sigma^f \bar{t} + i(a_1 \bar{x} + a_2 \bar{y})) \\ \bar{p}^f &= p^f(\bar{z}) \exp(\sigma^f \bar{t} + i(a_1 \bar{x} + a_2 \bar{y})) \\ \bar{\theta}^f &= \theta^f(\bar{z}) \exp(\sigma^f \bar{t} + i(a_1 \bar{x} + a_2 \bar{y}))\end{aligned}\quad (29)$$

Fluid region ($1 \leq z \leq 0$)

$$(D^2 - a_f^2)^2 W^f - a_f^2 R^f \Theta^f - Ha^2 D^2 W^f = \sigma^f (D^2 - a_f^2) W^f \quad (30)$$

$$(D^2 - a_f^2) \Theta^f + W^f M_1 R^f = \sigma^f Pr \Theta^f \quad (31)$$

Porous region ($-1 \leq z \leq 0$)

$$\frac{1}{\phi} (D^2 - a_m^2)^2 W^m - \frac{1}{Da} (D^2 - a_m^2) W^m - a_m^2 R^m \Theta^m - Ha_m^2 D^2 W^m \quad (32)$$

$$= \frac{\sigma^m}{\phi} (D^2 - a_m^2) W^m$$

$$(D^2 - a_m^2) \Theta^m + W^m M_2 R^m = \sigma^m M \epsilon_r Pr \Theta^m \quad (33)$$

$$\text{where, } a_f^2 = a_1^2 + a_2^2, \quad a_m^2 = (a_1^m)^2 + (a_2^m)^2 \quad (34)$$

Boundary conditions

$$W^f = DW^f = \Theta^f = 0 \text{ at } \bar{z} = 1 \quad (35)$$

$$W^m = DW^m = \Theta^m = 0 \text{ at } \bar{z} = -1 \quad (36)$$

Interference conditions at $\bar{z} = 0$

$$W^f = d_r W^m$$

$$W^f = d_r^2 DW^m \quad (37)$$

$$\phi (D^2 + a_f^2) W^f = d_r^3 (D^2 + a_m^2) W^m \quad (38)$$

$$\Theta^f = \sqrt{\epsilon_r} d_r^3 \Theta^m \quad (39)$$

$$D\Theta^f = \sqrt{\frac{d_r^5}{\epsilon_r}} D\Theta^m \quad (40)$$

$$\sigma^f DW^f - (D^2 - a_f^2) DW^f + 2a_f^2 DW^f = \frac{d_r^4 \sigma^m}{\phi} DW^m + \frac{d_r^4}{Da} DW^m \quad (41)$$

$$\begin{aligned}-\frac{d_r^4}{\phi} (D^2 - a_m^2) DW^m + \frac{2a_m^2 d_r^4}{\phi} DW^m \\ R_c^f = \min_{a^2} R^f(a^2, \lambda)\end{aligned}\quad (42)$$

where $D \equiv \frac{d}{dz}$

To find the critical Rayleigh number for instability, we let $\sigma^f = \sigma_r^f + i\sigma_i^f$ and the parameter values for which $\sigma_r^f = 0$, and relations of the dimensionless parameters can be obtained as

$$a_f = d_r a_m, \sigma_m = \frac{d_r^2}{\epsilon_r} \sigma^f \text{ and } R^f = \frac{d_r^4}{\epsilon_r^2 Da^2} R^m \quad (43)$$

2.6. Nonlinear stability analysis

Using the Energy method as given by Straughan [13]. Let us define V to represent the period of a cell in the porous layer and introduce the notation of norm in the inner product space $L^2(V)$ as follows:

$$\|f\|^2 = \int_V f_i f_i dV \text{ and } \langle f, g \rangle = \int_V f_i g_i dV \quad (44)$$

Now to obtain the condition of non-linear stability in the measure $L^2(V)$, multiply Eqs. (23) and (26) by \bar{u}_i^f and \bar{u}_i^m , and Eq. (24) and (27) by $\bar{\theta}^f$ and $\bar{\theta}^m$, and integrate over one period of the cell to get

$$E(\bar{t}) = \frac{1}{2} \|\bar{u}_i^f\|^2 + \frac{\lambda_1 Pr}{2} \|\bar{\theta}^f\|^2 + \frac{\lambda_2 \|\bar{u}_i^m\|^2}{2\phi} + \frac{\lambda_3 Pr \epsilon_r}{2} M \|\bar{\theta}^m\|^2 \quad (45)$$

$$\frac{dE}{d\bar{t}} = -\|\nabla \bar{u}_i^f\|^2 + R^f \langle \bar{\theta}^f, \bar{w}^f \rangle - Ha^2 \left(\|\bar{u}^f\|^2 + \|\bar{v}^f\|^2 \right) + \lambda_1 R^f \langle w^f M_1, \bar{\theta}^f \rangle \quad (46)$$

$$\begin{aligned} & -\lambda_1 \|\nabla \bar{\theta}^f\|^2 - \lambda_2 \frac{\|\nabla \bar{u}_i^m\|^2}{\phi} - \lambda_2 \frac{1}{Da} \|\bar{u}_i^m\|^2 + \lambda_2 R^m \langle \bar{\theta}^m, \bar{w}^m \rangle \\ & -\lambda_2 Ha_m^2 \left(\|\bar{u}^m\|^2 + \|\bar{v}^m\|^2 \right) + \lambda_3 R^m \langle M_2 \bar{w}^m, \bar{\theta}^m \rangle - \lambda_3 \|\nabla \bar{\theta}^m\|^2 \end{aligned} \quad (47)$$

$$\frac{dE}{d\bar{t}} = I - D$$

Let $\lambda_1 = \lambda$, $\lambda_2 = d_r^3$, $\lambda_3 = \lambda d_r^4$ as assumed by Hill and Straughan [8].

$$I = R^f \langle (M_1 \lambda + 1) \bar{w}^f, \bar{\theta}^f \rangle + d_r^3 R^m \langle (M_2 \lambda d_r + 1) \bar{w}^m, \bar{\theta}^m \rangle \quad (48)$$

$$\begin{aligned} D = & \|\bar{u}_i^f\|^2 + Ha^2 \left(\|\bar{u}_i^f\|^2 - \|\bar{w}^f\|^2 \right) + \lambda \|\nabla \bar{\theta}^f\|^2 + d_r^3 \frac{\|\nabla \bar{u}_i^m\|^2}{\phi} \\ & + d_r^3 \frac{1}{Da} \|\bar{u}_i^m\|^2 + d_r^3 Ha_m^2 \left(\|\bar{u}_i^m\|^2 - \|\bar{w}^m\|^2 \right) + \lambda d_r^4 \|\nabla \bar{\theta}^m\|^2 \end{aligned} \quad (49)$$

Introducing the maximization problem $1/R_E = \max_H (I/D)$, where H is the space of admissible function for solutions to Eqs.(22) -(27), it follows that

$$\frac{dE}{d\bar{t}} \leq -D \left(\frac{R_E - 1}{R_E} \right) \quad (50)$$

Using Poincaré's inequities, we can deduce that $D \geq kE$ for some constant k . After integration, we obtained $E(\bar{t}) \leq E(0)e^{-m\bar{t}}$ and $E(\bar{t}) \rightarrow 0$ as $\bar{t} \rightarrow \infty$, where $m = (R_E - 1)/R_E > 0$ and convergence is at least exponential.

The maximizing problem relates to the Euler-Lagrange equations are

Fluid region ($d \leq z \leq 0$)

$$2\Delta \bar{u}_i^f + R^f (\lambda M_1 + 1) \bar{\theta}^f \hat{k} - 2Ha^2 \bar{u}_i^f + 2Ha^2 \bar{w}^f \hat{k} = \omega_i^f \quad (51)$$

$$R^f (\lambda M_1 + 1) \bar{w}^f + 2\lambda \Delta_H \bar{\theta}^f = 0 \quad (52)$$

Porous region ($-d_m \leq z \leq 0$)

$$\frac{2d_r^3}{\phi} \Delta \bar{u}_i^m - \frac{2d_r^3}{Da} \bar{u}_i^m - 2d_r^3 Ha_m^2 \bar{u}_i^m + 2d_r^3 Ha_m^2 \bar{w}_i^m \hat{\mathbf{k}} + \quad (53)$$

$$d_r^3 R^m (\lambda M_2 d_r + 1) \bar{\theta}^m \hat{\mathbf{k}} = \omega_i^m$$

$$R^m (\lambda M_2 d_r + 1) \bar{w}_i^m + 2\lambda d_r \Delta_H \bar{\theta}^m = 0 \quad (54)$$

Now, again applying double curl to Eqs. (51) and (53), and eliminating the terms ω^f and ω^m , taking out the third component using normal modes, and obtained the following coupled ordinary differential equations

Fluid region ($1 \leq z \leq 0$)

$$(D^2 - a_f^2)^2 W^f - Ha^2 D^2 W^f - \frac{R^f}{2} (\lambda M_1 + 1) a_f^2 \Theta^f = 0 \quad (55)$$

$$\lambda (D^2 - a_f^2) \Theta^f + \frac{R^f}{2} (\lambda M_1 + 1) W^f = 0 \quad (56)$$

Porous region ($-1 \leq z \leq 0$)

$$\frac{1}{\phi} (D^2 - a_m^2)^2 W^m - \frac{1}{Da} (D^2 - a_m^2) W^m - Ha_m^2 D^2 W^m - \quad (57)$$

$$\frac{R^m}{2} (\lambda M_2 d_r + 1) a_m^2 \Theta^m = 0$$

$$\lambda d_r (D^2 - a_m^2) \Theta^m + \frac{R^m}{2} (\lambda M_2 d_r + 1) W^m = 0 \quad (58)$$

To determine the critical nonlinear Rayleigh number, defined as

$$R_{Nc}^f = \max_{\lambda} \min_{a^2} R^f(a^2, \lambda) \quad (59)$$

3. Numerical method

The Chebyshev Tau-QZ spectral method [14] is a powerful numerical technique used to solve linear stability problems, particularly eigenvalue problems arising in fluid dynamics and other areas of applied mathematics. It combines the Chebyshev spectral method, which offers high accuracy by expanding the solution in terms of Chebyshev polynomials, with the Tau method, which enforces boundary conditions by modifying the highest-order equations. The resulting generalized eigenvalue problem is then efficiently solved using the QZ algorithm, which is well-suited for large, non-symmetric systems. This method is especially effective for problems with complex boundary conditions and provides exponential convergence for smooth solutions.

4. Results and discussions

The couple ordinary differential equations are obtained and are solved using the Chebyshev Tau-QZ spectral method [14] and considering the physical values $\epsilon_r = 0.7$ and 0.9 , $Pr = 6$, $\phi = 0.79$, $Da = 5 \times 10^{-6}$, $M = 10$.

4.1. Validation

The validation of present study is validated with Hill and Straughan [8] when depth ratio $d_r = 0.100, 0.116$ and 0.15 , $\epsilon_r = 0.7$, $\epsilon_r = 0.7$, $Pr = 6$, $\phi = 0.79$, $Da = 5 \times 10^{-6}$, $M = 10$ and when taking Hartmann number $Ha = 0$ then present study found to be coincide with Hill and Straughan[8] as shown in Fig.2.

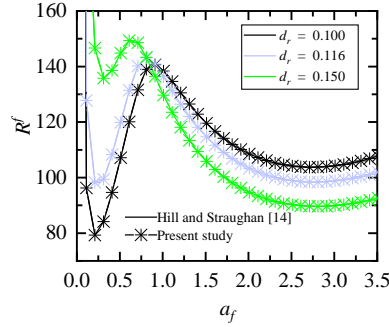


Fig.2. The validation of present work with Hill and Straughan [8] when $Ha = 0$

4.2. Marginal stability plots

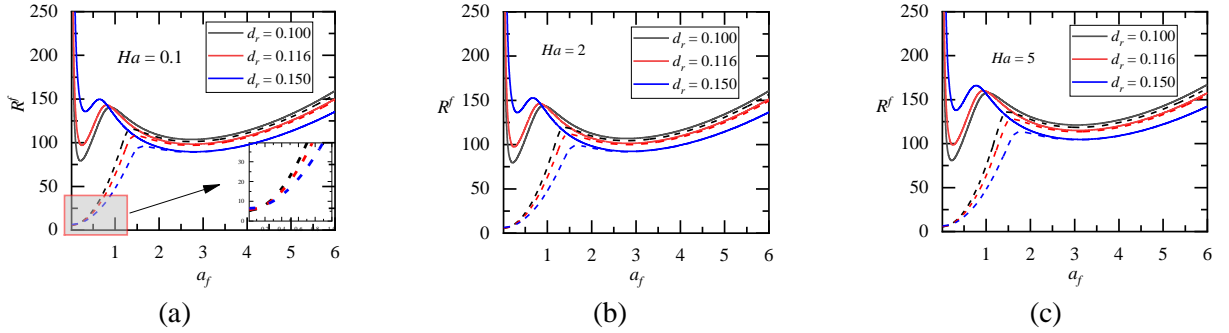


Fig.3. Marginal stability plots when (a) $Ha = 0.1$ (b) $Ha = 2$ (c) $Ha = 5$ at $\epsilon_T = 0.7$

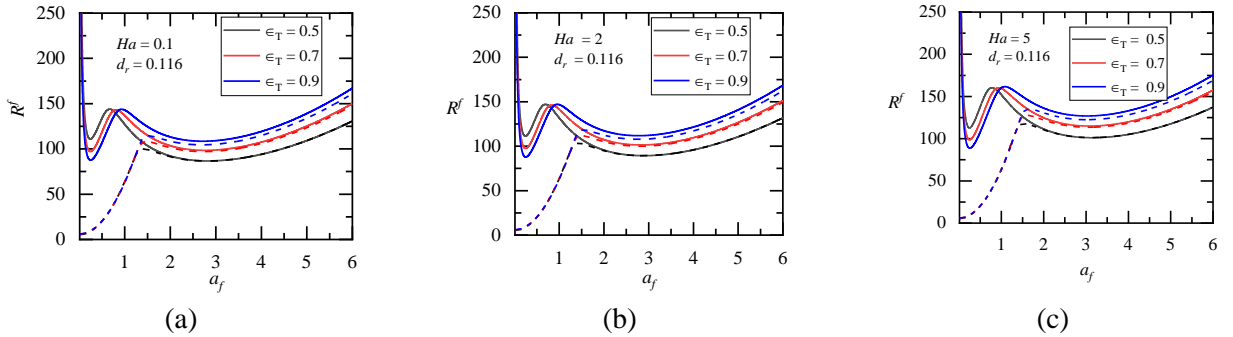


Fig.4. Marginal stability plots when (a) $Ha = 0.1$ (b) $Ha = 2$ (c) $Ha = 5$ at $d_r = 0.116$

Marginal stability plots delineate the boundary between stable and unstable regimes by identifying the critical Rayleigh number at which convection sets in under varying system parameters. Here, the depth ratio $d_r = d/d_m$. As d_r increases, indicating a relatively thicker fluid layer, the critical Rayleigh number also rises, reflecting greater system stability. A sharp drop in Rayleigh number at low wave numbers a_f signals fluid-dominated instability driven by buoyancy, while the minimum at intermediate a_f marks the most unstable mode, where both fluid and porous layers play significant roles. At higher a_f , the Rayleigh number rises steadily, indicating porous-dominated behaviour where the resistance of the porous medium suppresses convection. Nonlinear (dashed) curves lie below linear (solid) ones, capturing the earlier onset of instability due to nonlinear effects. It can be seen that as Hartmann number increases there is increase in upward shift of the marginal plots which shows the stabilizing effect of magnetic field as shown in Fig. 3. Similar, variation can also be seen in Fig. 4 with variation of ϵ_T when $Ha = 0.1, 2$ and 5 both have stabilizing effect ϵ_T which is the ratio of thermal conducting of fluid region to thermal conducting of porous region and Hartmann number.



Fig.5. Variation of critical Rayleigh number R_c^f with Hartmann number Ha when (a) $\epsilon_T = 0.7$ and (b) $\epsilon_T = 0.9$

The variation of critical Rayleigh number R_c^f with Hartmann number Ha when $\epsilon_T = 0.7$ and $\epsilon_T = 0.9$ with varying depth ratio d_r as shown in Fig.5 which clearly shown that stabilizing effect and with increasing in the ϵ_T also increases the R_c^f value which also shows the stabilizing effect. Physically, the Hartmann number represents the strength of the applied magnetic field. A higher Ha induces a stronger Lorentz force that damps velocity fluctuations, thereby stabilizing the flow and increasing the critical Rayleigh number as seen in linear stability shown with solid line whereas in nonlinear case R_c^f remains same but there is increase in R_c^f when $\epsilon_T = 0.9$ in nonlinear case.

4.3. Streamlines and Isotherms



Fig.6 (a) Streamline $\psi^f = \text{constant}$ and (b) Isotherm $\Theta^f = \text{constant}$ at $Ha = 0.5$ when $dr = 0.05$, $\epsilon_T = 0.7$



Fig. 7. (a) Streamline $\psi^f = \text{constant}$ and (b) Isotherm $\Theta^f = \text{constant}$ at $Ha = 5$ when $dr = 0.05$, $\epsilon_T = 0.7$

To illustrate the evolving instability patterns across different flow regimes, streamlines and isotherm plots are presented in Figs. (6) and (7) as part of the linear stability analysis. Here, curves denote streamlines ψ^f and curves denote isotherms Θ^f . The range of \bar{z} coordinate is taken from -1 to 1, whereas the range of \bar{x} coordinate is taken from 0 to $2\pi/a_c^f$. Each streamline and isotherms contour plots are plotted corresponding to the critical Rayleigh number and critical wave number, (R_c^f, a_c^f) of the corresponding given value. It is depicted in Fig. 6 and 7 streamlines and isotherms move away from bottom to top of the upper wall due to increase in the Hartmann number Ha from $Ha = 0.5$ to $Ha = 5$ when $d_r = 0.05$, $\epsilon_T = 0.7$. As the Hartmann number Ha increases from 0.5 to 5, the streamlines and isotherms shift upward toward the top wall. This occurs due to the increasing Lorentz force, which acts as a magnetic damping on the fluid motion, suppressing convection especially in the lower region. As a result, flow weakens near the bottom and concentrates near the top, leading to elongated

rolls and vertically stretched isotherms. This reflects reduced convective strength and enhanced thermal stratification, consistent with the stabilizing effect of a stronger magnetic field.

5. Conclusions

The key findings of this study are derived from both linear and nonlinear stability analyses conducted on a channel where a fluid overlies a porous medium. The system includes a vertically applied magnetic field, no-slip wall conditions, constant wall temperatures, and an interface condition at the fluid-porous boundary.

1. Instability is dominated by buoyancy in the fluid layer at low wave numbers, while at higher wave numbers, porous resistance stabilizes the flow. Increasing Hartmann number and thermal conductivity ratio further enhance stability, as reflected by the upward shift in marginal stability curves.
2. Hartmann number shows the stabilizing effect due to increases in critical Rayleigh number delays the onset of convection.
3. As depth ration increases due to increase in fluid region also shows stabilizing effect because critical Rayleigh numbers increase and ϵ_T also have stabilizing effect as R_c^f increases due to increase in thermal conductivity in fluid region which in turns delays the onset of convection.

Acknowledgement

One of the authors, Mr. Anil Kumar (Reg. No. MA21S55006166), is very thankful to the MHRD Government of India for the doctoral fellowship.

Authors Declarations

Conflicts of Interest

The authors have no conflicts to disclose.

Data Availability

The availability of the data can be accessed, which supports this study from the corresponding author upon reasonable request.

References

- [1] D. A. Nield, Onset of convection in a fluid layer overlying a layer of a porous medium. *Journal of Fluid Mechanics*, 81(3) (1977) 513-522.
- [2] D. A. Nield, The limitations of the Brinkman-Forchheimer equation in modeling flow in a saturated porous medium and at an interface. *International Journal of Heat and Fluid Flow*, 12(3) (1991) 269-272.
- [3] Chen, F. and Chen, C.F., Convection in superposed fluid and porous layers. *Journal of Fluid Mechanics*, 234, (1992) 97-119.
- [4] Das, D.B. and Lewis, M., Dynamics of fluid circulation in coupled free and heterogeneous porous domains. *Chemical engineering science*, 62(13) (2007)3549-3573.
- [5] M. Mu, and J. Xu, A two-grid method of a mixed Stokes–Darcy model for coupling fluid flow with porous media flow. *SIAM journal on numerical analysis*, 45(5) (2007)1801-1813.
- [6] B. Rivière, Analysis of a discontinuous finite element method for the coupled Stokes and Darcy problems. *Journal of Scientific Computing*, 22(1-3) (2005)479-500.
- [7] A.A. Hill, and B. Straughan, Poiseuille flow in a fluid overlying a highly porous material. *Advances in water resources*, 32(11) (2009)1609-1614.
- [8] A.A. Hill, and B. Straughan, Global stability for thermal convection in a fluid overlying a highly porous material. *Proceedings of the Royal Society A: Mathematical, Physical and Engineering Sciences*, 465(2101) (2009)207-217.
- [9] A.A. Hill, and B. Straughan, Poiseuille flow in a fluid overlying a porous medium. *Journal of Fluid Mechanics*, 603 (2008) 137-149.
- [10] A.A. Hill, and M. Carr, Sharp global nonlinear stability for a fluid overlying a highly porous material. *Proceedings of the Royal Society A: Mathematical, Physical and Engineering Sciences*, 466(2113) (2010)127-140.

- [11] A. Kumar, D. Bhargavi, & P.G. Siddheshwar, Magneto-hydro-convective instability in a saturated Darcy–Brinkman medium with viscous dissipation. *Eur. Phys. J. B* 97, (2024) 107.
- [12] S. Chandrasekhar, *Hydrodynamic and hydromagnetic stability*, Courier Corporation, 2013.
- [13] B. Straughan, *The energy method, stability, and nonlinear convection* (Vol. 91), Springer Science & Business Media, 2013.
- [14] J.J. Dongarra, B. Straughan, and D.W. Walker, Chebyshev tau-QZ algorithm methods for calculating spectra of hydrodynamic stability problems, *Appl. Numer. Math.*, 22(4), (1996) 399-434.